Multiphase Flow in Porous Media: Cake Formation During Extreme Drilling Processes

M.A. Kabir and Isaac K. Gamwo

Abstract The successful completion of a wellbore requires a low-permeable filter cake to be deposited on the wellbore walls to seal the porous formation exposed by the drill bit. The filtration processes triggered by the differential pressure between the drilling fluid in the borehole and the pore spaces of formation rocks are well known in both drilling operations and, of greater importance, in the subsequent production of oil. The filter cake acts as a barrier to prevent excessive drilling fluid loss into formation, and invasion of formation fluid. The presence of a filter cake also provides wellbore stability and reduces damage to the formation. Understanding cake formation and fluid flow through porous media is necessary for a successful drilling process. This need becomes even more important during extreme drilling, when pressure and temperature may exceed 35,000 psi and 500 °F. This work presents our effort to simulate the fluid flow and cake formation in extreme drilling processes. Earlier investigations were focused on single-phase flow phenomena in porous media; recent studies have emphasized multiphase (thermo-fluid) flow in porous media to closely mimic the actual drilling fluid composed of fine particles and viscous fluid. In the present study, the Eulerian–Eulerian approach for multiphase flow is employed to evaluate the fluid flow and cake formation patterns during ultra-deep drilling at high-temperature, high-pressure conditions. The rheology of the fluid has been published previously [14] and is repeated here for completeness. Two competitive sub-models were considered: the power-law and the Herschel–Bulkley models. The Herschel–Bulkley rheological model appears superior and best describes the non-Newtonian rheological behavior of drilling fluid due to the yield stress term present in this model.

M.A. Kabir · I.K. Gamwo (✉)
National Energy Technology Laboratory, United States Department of Energy,
Research & Innovation Center, Pittsburgh, PA 15236, USA
e-mail: gamwo@netl.doe.gov

Present Address:
M.A. Kabir · I.K. Gamwo
SABIC Innovative Plastics, Polymer Processing Development Center, Pittsfield, MA, USA

Keywords Drilling fluid · Multiphase flow · Filter cake formation · Computational fluid dynamics · Deep drilling

1 Introduction

Drilling fluids play a vital role in drilling operations and perform several important tasks: (a) helping to reduce friction and wear on the drilling bit, (b) transporting the drilled solids, (c) maintaining a favorable pressure difference between the wellbore and the rock formation, (d) cooling the cutters to maintain the temperature below critical, (e) generating a filter cake on the wellbore wall to minimize incursion of drilling fluids into the formation [1, 3, 5, 7, 36, 38].

Additionally, loss of drilling fluids during operations through hydrocarbon-bearing formations is expected to be minimized. The drilling fluid filtrates can lead to formation damage because of rock wettability changes, fines migration, drilling fluid solids plugging, and formation water chemistry incompatibilities [4]. The filtration properties are one of the most important characteristics of all drilling fluids. The invasion of filtrate into the formation can substantially reduce the permeability of the region near the wellbore and may occur through several mechanisms: clay swelling, particles pore plugging, particles migration, and water blocking. Moreover, the nature and thickness of the filter cake deposited on the borehole wall may cause a pressure differential that can lead to sticking [2, 4, 14, 39].

Drilling fluids are designed to exhibit non-Newtonian properties. The drilling mud prevents the rock cuttings from settling at the bottom hole under static conditions as the drilling fluid circulation is stopped, (e.g., to replace the drilling pipe or bit). Yet, at high shear rates when drilling operation resumes, the drilling fluid is expected to flow like a viscous paste removing drilled rock cuttings from the well bottom and carry them to the surface. Accurate modeling of the drilling process and filter cake formation is important so that reliable multiphase flow mathematical models may be developed; these models would predict the drilling fluid flow rate necessary to remove cuttings that would otherwise cause severe problems during drilling such as high drag and torque.

Literature review [1, 5, 10, 27] shows that little research has been carried out modeling on deep drilling processes and cake formation to predict multiphase flow behavior. Recently, the extreme drilling process attracted the attention of fluid researchers due to the drilling fluid vital role in rock cutting removal and in filter cake formation.

In this study, we utilized the Eulerian–Eulerian multiphase flow model to evaluate the drilling fluid flow pattern and filter cake formation patterns for two rheological models: the power-law model and the Herschel–Bulkley model. The parameters in the Herschel–Bulkley rheological model best describe the non-Newtonian rheological behavior of drilling fluid. This includes a yield stress that would allow cuttings to float under static conditions. Our simulations of the

flow patterns indicate that the Herschel–Bulkley model is a more accurate model of rheological behavior, and it exhibits better cutting removal performance.

This investigation was further extended to study the effect of differential pressure on filter cake thickness. The ability to optimize filter cake characteristics is extremely useful [10]. The presence of filter cake reduces both formation damage and fluid loss. With thicker cake, the effective diameter of the hole is reduced and problems may arise, such as excessive torque when rotating the drill string and excessive drag when pulling it. Here we have demonstrated a correlation between cake thicknesses and pressure drop by varying the pressure drop from 250 psi (1.72 MPa) to 1000 psi (6.89 MPa) with incremental pressure drop of 250 psi (1.72 MPa) under extreme drilling conditions.

Most of the previous studies have been carried out with Newtonian, single-phase and isothermal conditions for the shallow drilling process. Here, we have performed initial research on the computational fluid dynamics (CFD) modeling and simulations of the flow pattern and filter cake formation resulting in multiphase flow in porous media at extremely high-pressure and high- temperature (up to 25,500 psi or 175.8 MPa and 170 °C) drilling process. The drilling fluid was treated as a two-phase system with solid (45 µm) particles suspended in a non-Newtonian fluid where fluid phase was modeled using the power-law model without yield stress and the Herschel–Bulkley model with yield stress. The CFD code ANSYS Fluent was used for solving mass, momentum, and energy equations for fluid and solid phases where a Eulerian–Eulerian multiphase model was employed.

In this chapter, we have used three main interlinked solution aspects to modeling [10] the filter cake formation in multiphase flow in porous media for a deep drilling process (25,000 psi or 172.4 MPa and 170 °C). The solution aspects used are (i) the Eulerian–Eulerian multiphase fluid flow model in the pipe as well as in the annulus between the pipe and the borehole, (ii) the filter cake deposition model by retaining of the annulus fluid particles at the formation cavity during the seepage, and (iii) the drilling fluid seepage into the formation during and after the cake formation.

Our main focus was to numerically study the effect of two rheological models on the fluid flow pattern and filter cake formation at high temperatures and high pressures utilizing CFD tools. Numerical predictions were performed for a range of overbalance differential pressure from 250 psi (or 1.72 MPa) to 1250 psi (or 8.62 MPa) with incremental pressure of 250 psi (or 1.72 MPa) to study the effect of differential pressure over cake thickness.

2 Governing Equations—Multiphase Flow in Porous Media

The dynamics of solids in fluid media have a large effect on various flow phenomena such as density, viscosity, and pressure. Thus, the hydrodynamics of solids must be modeled correctly [6]. The Eulerian approach is preferred over the

Lagrangian due to the large volume fraction of solids in the drilling fluid. In the Eulerian approach, fluid and solid phases are treated as interpenetrating continua, and momentum and continuity equations are defined for each phase [12]. Therefore, the Eulerian–Eulerian multiphase fluid model has been used to simulate fluid flow and filter cake formation for deep drilling process conditions. The Eulerian model solves a set of n momentum and continuity equations for each phase. Coupling is achieved through the pressure and interphase exchange coefficients. The manner in which this coupling is handled depends upon the type of phases involved. For granular flows, properties are obtained by applying kinetic theory. Mass transfer between the phases is negligible and, therefore, ignored here. The momentum equation for the solid phase differs from the equation used for the fluid phase, since the former contains a solids pressure [12, 17, 18, 28]. Lift and virtual mass forces are assumed to be negligible in the momentum equations. Details of the rheological models used in this study can be found elsewhere [14].

2.1 Modeling Fluid Flow in the Annulus

Multiphase equations for modeling the flow of steady, laminar, non-isothermal, incompressible fluid are given in the following sections [6, 12, 17, 18, 28].

2.1.1 Conservation of Mass

$$\text{For liquid,} \quad \nabla.(\alpha_l v_l) = 0 \tag{1}$$

$$\text{For solids,} \quad \nabla.(\alpha_s v_s) = 0 \tag{2}$$

where α is the volume fraction and subscripts l and s denote liquid and solid phases, respectively. Moreover, $\alpha_l + \alpha_s = 1$ must be satisfied. v_l and v_s are the velocities of the solid and liquid phases, respectively.

2.1.2 Momentum Balance

Liquid Phase

The momentum equation for the liquid phase in a solid–liquid system [6, 12, 17, 18, 28] is as follows:

$$\underbrace{\nabla.(\alpha_l \rho_l \vec{v}_l \vec{v}_l)}_{\text{Convective}} = -\underbrace{\alpha_l \nabla p}_{\text{Pressure}} + \underbrace{\nabla.\overline{\tau_1}}_{\text{Stress}} + \underbrace{\alpha_l \rho_l \vec{g}}_{\text{Body}} - \left\{ \left(\underbrace{K_{sl}(\vec{v}_l - \vec{v}_s)}_{\text{Forces Exchange}} \right) \right\} \tag{3}$$

where ρ_l and ρ_s are the densities of liquid and solid phases, respectively.

To address non-Newtonian behavior of the liquid phase in the multiphase drilling fluid, we have used the power-law model input parameters in the simulation [10, 12].

For the fluid, the stress tensor, $\overline{\tau}_l$, is related to the fluid strain rate tensor, $\overline{\dot{\gamma}}_l = \nabla \vec{v}_l + (\nabla \vec{v}_l)^{tr}$, by:

$$\overline{\tau}_l = \alpha_l \tau \overline{\dot{\gamma}}_l + \alpha_l \left(\lambda_l - \frac{2}{3} \tau \right) \nabla . \vec{v}_l \overline{I} \tag{4}$$

where $\tau = \tau_o + k |\overline{\dot{\gamma}}_l|^{n-1}$ or $\tau = k |\overline{\dot{\gamma}}_l|^{n-1}$ and $|\overline{\dot{\gamma}}_l|$ is the magnitude of the strain rate tensor defined as $|\overline{\dot{\gamma}}| = \sqrt{\frac{1}{2} \sum_i \sum_j \dot{\gamma}_{ij} \dot{\gamma}_{ji}}$, τ_o is the yield stress, and k and n are consistency factor and power-law exponent, respectively [10, 12, 16].

Solid Phase

The momentum equation for the solid phase in a solid–liquid system [6, 12, 17, 18, 28] is:

$$\nabla . (\alpha_s \rho_s \vec{v}_s \vec{v}_s) = -\alpha_s \nabla p - \underbrace{\nabla p_s}_{} + \nabla . \overline{\tau}_s + \alpha_s \rho_s \vec{g} + \{ (K_{ls}(\vec{v}_l - \vec{v}_s)) \} \tag{5}$$
$$\text{Solid Pressure}$$

The solids pressure p_s, stress $\overline{\tau}_s$, and viscosity μ_s are determined by particle fluctuations, the kinetic energy associated with these fluctuations, and the granular temperature Θ.

The stress-strain relationship for the solid phase s is:

$$\overline{\tau}_s = \alpha_s \underbrace{\mu_s \overline{\dot{\gamma}}_s}_{} + \alpha_s \left(\underbrace{\lambda_s}_{} - \frac{2}{3} \mu_s \right) \nabla . \vec{v}_s \underbrace{\overline{I}}_{} \tag{6}$$
$$\text{Shear stress} \quad \text{Bulk viscosity} \quad \text{Unit tensor}$$

where solid strain rate tensor $\overline{\dot{\gamma}}_s = \nabla \vec{v}_s + (\nabla \vec{v}_s)^{tr}$.

Interaction forces are considered here to account for the effects of other phases and are reduced to zero for single-phase flow [6, 12]. The momentum exchange coefficients are indistinguishable ($K_{ls} = K_{sl}$)

$$K_{sl} = \frac{\alpha_s \rho_s f}{T_s^p} \tag{7}$$

This function and these coefficients are suitable for drilling process modeling where re-circulating multiphase fluids contain high solid fraction.

Here, T_s^p is the particulate relaxation time and f is the model dependent drag function.

The relaxation time is expressed as

$$T_s^p = \frac{\rho_s d_s^2}{18\mu_l} \tag{8}$$

where d_s is the solid particle diameter.

When the Syamlal–O'Brien Drag function f [6, 12] is used:

$$f = \frac{C_D Re_s \alpha_l}{24 v_{r,s}^2} \tag{9}$$

The relative Reynolds number R_{e_s} can be written as follows [6, 12]:

$$R_{e_s} = \frac{\rho_l d_s |\vec{v}_s - \vec{v}_l|}{\mu_l} \tag{10}$$

The drag function f includes a drag coefficient C_D and the relative Reynolds number R_{e_s}; however, the drag function differs among the exchange-coefficient models. For the drilling process, multiphase drilling fluid with a high solid fraction continuously cycles through the drill assembly and carries away debris produced by the drilling process.

In the Syamlal–O'Brien model, the drag function of Dalla Valle is used [6, 12] where $v_{r,s}$ is the terminal velocity correlation:

$$C_D = \left[0.63 + \frac{4.8}{\sqrt{Re_s/v_{r,s}}} \right]^2 \tag{11}$$

The terminal velocity correlation $v_{r,s}$ for solid phase has the following form:

$$v_{r,s} = 0.5 \left(A - 0.06 Re_s + \sqrt{(0.06 Re_s)^2 + 0.12 Re_s (2B - A) + A^2} \right) \tag{12}$$

where

$A = \alpha_l^{4.14}$
$B = 0.8 \alpha_l^{1.28}, \quad \alpha_l \leq 0.85$
$B = \alpha_l^{2.65}, \quad \alpha_l > 0.85$

This correlation is based on measurements of the terminal velocities of particles in fluidized or settling beds where high solid volume fractions, similar to solid volume fractions in drilling fluids, are encountered.

The solid pressure P_s is composed of a kinetic term (first term), a particle collisions term (second terms) and a friction term (3rd term) [6, 12]:

$$P_s = \alpha_s \rho_s \Theta_s + 2\rho_s(1 + e_{ss})\alpha_s^2 g_{0,ss}\Theta_s + F_r \frac{\left(\alpha_s - \alpha_{s,\min}\right)^n}{\left(\alpha_{s,\max} - \alpha_s\right)^p} \tag{13}$$

Both kinetic and collision terms are dependent on the granular temperature Θ. The term e_{ss} is the particle–particle coefficient of restitution (taken here to be $e_{ss} = 0.9$; this choice is consistent with values reported in the literature under similar simulation conditions), $g_{0,}$ is the radial distribution function. This is a correction factor (the non-dimensional distance between spheres) that modifies the probability of collisions between particles when the granular phase becomes dense. The friction is included in this study because the solid volume fraction is relatively high, which may give rise to friction. In this work, the friction pressure is modeled using the semi-empirical model proposed by Johnson et al. [19], where $\alpha_{s,\min}$ and $\alpha_{s,\max}$ are the minimum and maximum packing respectively; $\alpha_{s,\min}$, assumed to be 0.5, is the solid concentration when friction stresses becomes important. The values of empirical materials constants F_r, n, and p are taken to be 0.5, 2.0, and 5.0 respectively following other investigators [19].

2.1.3 Energy Equation

To describe the conservation of energy in Eulerian multiphase applications, a separate steady-state enthalpy equation can be written for each phase q (liquid or solid) [6, 12] as follows:

$$\nabla \cdot \left(\underbrace{\alpha_q \rho_q \overrightarrow{u}_q h_q} \right) = \underbrace{\overline{\overline{\tau_q}} : \nabla \overrightarrow{u}_q} - \underbrace{\nabla \cdot \overrightarrow{q}_q} + \sum_{p=1}^{n} \left(\underbrace{\overrightarrow{Q}_{pq}} \right) \tag{14}$$

where h_q is the specific phase enthalpy, $\overrightarrow{q_q}$ is the heat flux, and $\overrightarrow{Q}_{pq}$ is the intensity of heat exchange between phases.

2.1.4 Granular Temperature

The granular temperature for the solid phase must be specified for particulate viscosities. We used a partial differential equation, which was derived from the transport equation by neglecting convection and diffusion. It takes the following form [6, 12]:

$$0 = (-p_s \bar{\bar{I}} + \overline{\overline{\tau_s}}) : \nabla \overrightarrow{v_s} - \gamma_{\Theta_s} + \phi_{ls} \tag{15}$$

where $(-p_s\bar{I} + \overline{\tau_s}) : \nabla\vec{v}_s$ is the generation of energy by the solid stress tensor, γ_{Θ_s} is the collisional dissipation of energy, and ϕ_{ls} is the energy exchange between the fluid and the solid phase.

The collisional dissipation of energy, γ_{Θ_s}, represents the rate of energy dissipation within the solid phase due to collisions between particles. The term is represented by the following expression derived by Lun [26]:

$$\gamma_{\Theta_s} = \frac{12(1 - e_{ss}^2)g_{0,ss}}{d_s\sqrt{\pi}}\rho_s\alpha_s^2\Theta_s^{3/2} \tag{16}$$

The transfer of the kinetic energy of random fluctuations in particle velocity from the solid phase to the liquid phase is represented by ϕ_{ls}:

$$\phi_{ls} = -3K_{ls}\Theta_s \tag{17}$$

The radial distribution function $g_{0,ss}$ is modeled as follows [6, 8, 12]:

$$g_{0,ss} = \left[1 - \left(\frac{\alpha_s}{\alpha_{s,\max}}\right)^{1/3}\right]^{-1} \tag{18}$$

(The symbols are defined in Table 1.)

where $\alpha_{s,\max}$ is the maximum packing, assumed here to be 0.63.

The viscosity for the solids stress tensor is the sum of the collisional, kinetic, and frictional viscosity elements:

$$\mu_s = \mu_{s,col} + \mu_{s,kin} + \mu_{s,fr} \tag{19}$$

The collisional element of viscosity is modeled as follows [6, 8, 12, 15]:

$$\mu_{s,col} = \frac{4}{5}\alpha_s^2\rho_s d_s g_{0,ss}(1 + e_{ss})\left(\frac{\Theta_s}{\pi}\right)^{1/2} \tag{20}$$

The kinetic part of viscosity is modeled using the equation of Syamlal [12]:

$$\mu_{s,kin} = \frac{\alpha_s d_s \rho_s\sqrt{\Theta_s\pi}}{6(3 - e_{ss})}\left[1 + \frac{2}{5}(1 + e_{ss})(3e_{ss} - 1)\alpha_s g_{o,ss}\right] \tag{21}$$

Shear stress includes bulk viscosity, λ_s, which in granular flows is related to the particles' resistance to compression and expansion. The bulk viscosity expression of Lun et al. [26] was used in this simulation:

$$\lambda_s = \frac{4}{3}\alpha_s\rho_s d_s g_{0,ss}(1 + e_{ss})\left(\frac{\Theta_s}{\pi}\right)^{1/2} \tag{22}$$

Table 1 Definition of symbols

Symbol	Description	Units
Alphabetic		
C_D	Drag coefficient	Dimensionless
d_s	Solid particle diameter	m
e	Coefficient of restitution	Dimensionless
g	Gravitational acceleration	m/s^2
g_0	Radial distribution function	Dimensionless
k	Consistency index	Dimensionless
K	Interphase exchange coefficient	Dimensionless
K_p	Porous media permeability	m^2
P	Pressure (fluid)	Pa
R_e	Relative Reynolds number	Dimensionless
t	Time	s
D_p	Porous media mean particle diameter	m
F_r	Materials constant in Eq. 17 (=0.5)	Dimensionless
p	Materials constant in Eq. 17 (=5.0)	Dimensionless
n	Materials constant in Eq. 17 (=2.0)	Dimensionless
n_i	Flow index	Dimensionless
Greek letters		
α	Volume fraction (solid or liquid)	Dimensionless
ρ	Density	kg/m^3
Θ	Granular temperature	m^2/s^2
$\bar{I}$	Unit stress tensor	Dimensionless
γ_{Θ_s}	Collision dissipation of energy	$kg/s^3\ m$
$\bar{I}_{2D}$	Second invariant of deviatoric stress tensor	Dimensionless
λ	Bulk viscosity	Pa s
μ	Shear viscosity	Pa s
$\vec{v_s}$	Solid velocity vector	m/s
$\vec{v_l}$	Fluid velocity vector	m/s
v	Seepage velocity	m/s
$\bar{\tau}$	Stress tensor	Pa
ε	Porous media void volume fraction	Dimensionless
Subscripts		
col	Collision	
fr	Friction	
kin	Kinetic	
l	Liquid phase	
Max, min	Maximum, minimum value	
q	Either liquid or solid phase	
s	Solid phase	

When the solids volume fraction is near the packing limit, the friction between particles is important. The friction element of the shear viscosity can be defined using Schaeffer's expression:

$$\mu_{s,fr} = \frac{p_{sfr} \sin \theta}{2\sqrt{I_{2D}}} \tag{23}$$

where θ is the angle of internal friction and I_{2D} is the second invariant of the deviatoric stress tensor [12].

2.2 Modeling Fluid Flow in Porous Rock Formation

The multiphase fluid flow through the porous rock is modeled using an extension of Darcy's law for multiphase flow, also referred to as the Ergun equation for laminar flow or the Blake–Kozeny equation. This equation reads

$$\nabla P = -\frac{\mu}{K_p} v \tag{24}$$

where v is the seepage fluid velocity in the formation and μ the fluid dynamic viscosity. The porous media permeability, K_p, is given below in terms of formation porosity (ε) and the porous media mean pore size (D_p). Here, we set a formation void fraction of 0.2 following Parn-anurak [31]:

$$K_p = \frac{D_p^2}{150} \frac{\varepsilon^3}{(1-\varepsilon)^2} \tag{25}$$

The differential pressure in between the porous media formation and annulus was maintained at 500 psi (3.4 MPa).

2.3 Mechanism of Filter Cake Formation in the Porous Rock Surface

Figure 1 displays a simplified diagram of the drilling process model for oil and gas reservoirs. In our simulation, we zoomed in the bottom drilling zone to capture detailed phenomena occurring during the drilling process. The filter cake is shown on the vertical wellbore wall. The particulate multiphase drilling fluid is pumped-down into the drilling zone through a drilling pipe where drilling fluid interacts with rock debris. As particulate-laden drilling fluid flows upward to the surface through the annulus in between the walls of the well and the drill string,
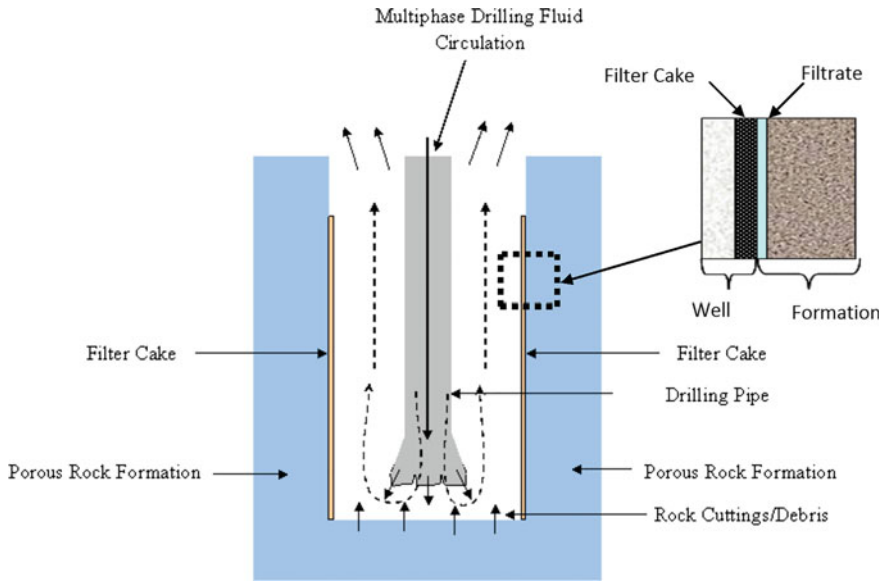
Fig. 1 Schematic diagram of the drilling process model. "Reprinted from *Asia-Pac. Journal of Chemical Engineering, 10, 809, 2015-Gamwo and Kabir, with permission from John Wiley and Sons, September 12, 2016*"

differential pressure causes filter cake to form on the porous rock reservoir surface as shown in Fig. 1.

As the annulus pressure exceeds the formation pressure, the overbalance pressure forces the fluid phase of the drilling fluid through the porous formation and deposits particles on the porous rock surface in the form of filter cake. Fluid seepage in the porous rock surface is related to the rock resistance, fluid viscosity, and differential pressure—this relationship can be described by Darcy's Law [5, 10, 13, 31]. As time progresses, filter cake will grow on the rock surface; therefore, filter cake itself will also resist fluid permeation into porous rock formations and, hence, fluid permeation will decrease. The resistance from filter cake can be related to the concentration of mass loading per unit area (kg/m^2) and specific resistance (m/kg). The filter cake builds up to a maximum thickness, which is determined by particle characteristics and fluid shear [10, 13].

2.4 Two-Dimensional Wellbore Model

A two-dimensional (2-D) wellbore model of a vertical well was created and meshed with Gambit as shown in Fig. 2. Symmetry along the central axis was assumed. To simulate the drilling process, multiphase particulate ($\alpha_s = 0.2$) drilling fluid was pumped into the model inlet, and multiphase particulate ($\alpha_s = 0.8$) rock debris was
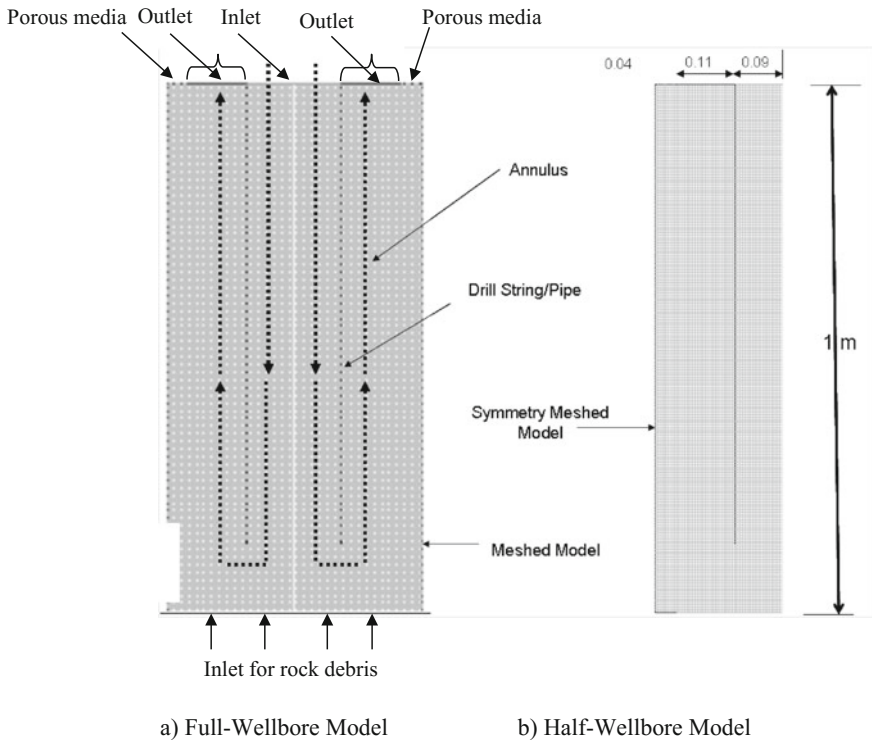
a) Full-Wellbore Model   b) Half-Wellbore Model

Fig. 2 Meshed vertical wellbore model. "Reprinted from *Asia-Pac. Journal of Chemical Engineering, 10, 809, 2015*-Gamwo and Kabir, with permission from John Wiley and Sons, September 12, 2016"

pushed from the bottom inlet. The model inlet represents drilling fluid pumping in, and the bottom inlet represents rock debris that accumulates during drilling. The solid wall represents the drill string surface. A porous medium with solid volume fraction of 0.8 next to the drill string represents the vertical rock formations on which filter cake builds up. The pressure and temperature are 25,500 psi (175.8 MPa) and 170 °C, respectively, for deep drilling conditions. The formation pressure and temperature were maintained at 25,000 psi (172.4 MPa) and 170 °C to mimic real-world drilling scenarios. Multiphase particulate non-Newtonian drilling fluids were pumped into the drilling zone where the drilling fluids mixed with rock particles. The particle-laden drilling fluid then flowed upwardly, back to the surface, through the annulus between the walls or sides of the wellbore and the drill string. A variety of drilling fluids exist, and, as mentioned earlier, the circulation of the drilling fluid, among others, lubricates the drill bit, removes cuttings from the wellbore as they are produced, exerts hydrostatic pressure on pressurized fluid contained in formations, and seals off the walls of the wellbore so that the fluid is not lost in the permeable subterranean zones [32].

2.4.1 Initial and Boundary Conditions

In our modeling and simulations, the wellbore was initially filled with multiphase particulate drilling fluid or mud while the bottom portion of the drilling zone was filled with rock debris as shown in Fig. 3. The non-Newtonian fluid properties with yield stress were given for the liquid phase, and the granular properties were given for solid particles. The density of the liquid phase was 999 kg/m^3, whereas yield stress (τ_o), consistency (k) index, and power-law (n) index were 3 Pa, 0.1238 Pa.s^n, and 0.67 respectively [10, 16]. The solid phase density was set at 2350 kg/m^3. In this study, the particle size in the drilling fluid was 45 μm for wellbore simulation. The domain was discretized with grid where the flow domain was divided into finite surfaces. As mentioned earlier, axisymmetry was assumed for the modeling the drilling process. Several trials were made (from 5500 to 11,000 meshes) to verify grid independent results from CFD simulations. The half-wellbore model consists of 9600 quadrilateral mesh cells with uniform size of 0.5 cm × 0.5 cm for a vertical well. The dimension of the porous media formation in the model was 4 cm × 100 cm, and the porous media formation pressure and temperature were maintained at 25,000 psi (172.4 MPa) and 170 °C for deep drilling conditions.

Our extensive literature review revealed very few experimental and numerical studies have been carried out on the multiphase flow pattern and filter cake formation in deep drilling processes; we therefore had few studies with which to
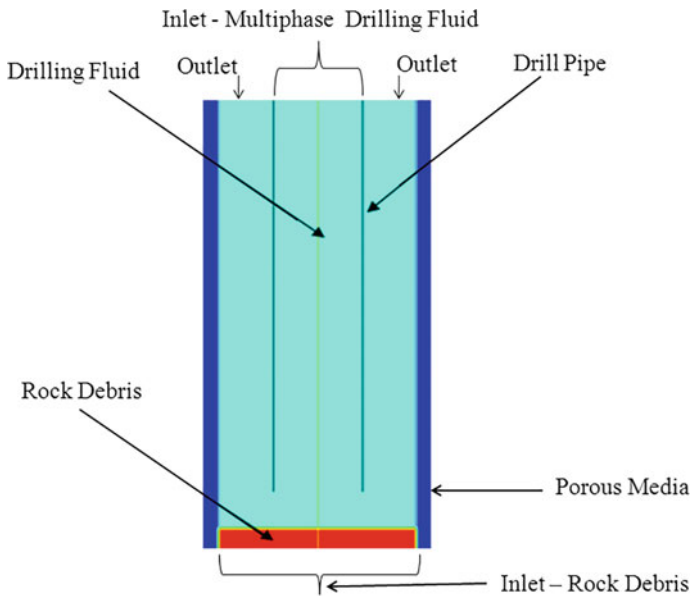

Fig. 3 Initial solid distribution in the vertical well. "Reprinted from *Asia-Pac. Journal of Chemical Engineering, 10, 809, 2015-Gamwo and Kabir, with permission from John Wiley and Sons, September 12, 2016*"

validate our CFD modeling results [5, 10, 16, 31, 32, 34, 35, 37]. To compensate, a single pressure vertical-linear multiphase filtration process was modeled to validate our CFD model. To experimentally validate the filter cake thickness, we previously compared experimental filter cake data of iron ore suspension with CFD simulation results. The analytical, experimental, and numerical results of filter cake heights in multiphase flow porous media compared reasonably well, as described in detail elsewhere [24].

3   Results and Discussion

The simulated initial and boundary conditions described in the previous section (Sect. 2.4.1) are similar to conditions found in field drilling operations [1, 3, 5, 7, 10, 16, 27, 31, 32, 34–38, 40]. The details of these conditions for deep drilling simulations are provided in Table 2.

The deep drilling process was simulated by setting high-pressure (25,500 psi or 175.8 MPa) and high-temperature (170 °C) conditions at the inlet and bottom portion of the well. The differential pressure between wellbore and porous media was maintained at 500 psi (or 3.45 MPa); however, simulations were performed on a range of overbalance differential pressures at 250 psi (or 1.72 MPa), 500 psi (or 3.45 MPa), 750 psi (or 5.17 MPa), 1000 psi (or 6.89 MPa), and 1250 psi (or 8.62 MPa) to study the effect of differential pressure on fluid flow pattern and cake formation.

The bottom portion of the simulated well was maintained at the same pressure and temperature as that of inlet. It was assumed that the pressure and temperature variations over a 1 m long model are negligible. In this study, reservoir formation porosity was assumed to be 0.2. Similar porosity value has been used by other researchers [31].

Table 2 Initial conditions and fluid/formation properties for a vertical well

	Well depth
Inlet pressure (drilling fluid/top) (psi or MPa)	25,500 or 175.8
Pressure (bottom) (psi or MPa)	25,500 or 175.8
Outlet pressure (psi or MPa)	25,000 or 172.4
Formation pressure (porous media) (psi or MPa)	25,000 or 172.4
Particle size (μm)	45
Formation porosity (dimensionless)	0.2
Temperature (°C)	170
Solid fraction (drilling fluid/top) (dimensionless)	0.2
Solid fraction (rock/bottom) (dimensionless)	0.8
Particle density (kg/m^3)	2350
Fluid density (kg/m^3)	999

The wellbore was maintained at a higher pressure than the surrounding porous media to mimic actual overbalance drilling conditions in the well. The differential pressure in the annulus forces fluid through the porous media and deposits solid particles in the form of filter cake on the porous rock surface, as shown in Fig. 4a; filter cake is indicated by a higher volume of solids at the wall. The filter cake grows on the wall in a process similar to simple soil consolidation where differential pressure initially forces some drilling fluid into the formation, and the solids present in the drilling fluid clog the pores of the formation and accumulate against the wall under appropriate conditions. As the pressure difference between the wellbore and the formation forces the filter cake to consolidate, the fluid phase (filtrate) invades the formation. The solid particles become more tightly packed, reducing the permeability of the growing cake and, hence, the fluid moves into the formation [5].
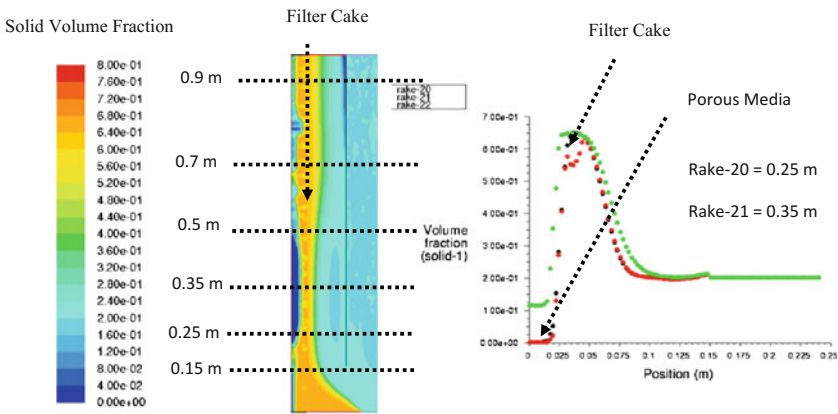
a) Qualitative solid fraction of well (half).

b) Solid fraction at different well heights of 0.25 m, 0.35 m and 0.5 m.
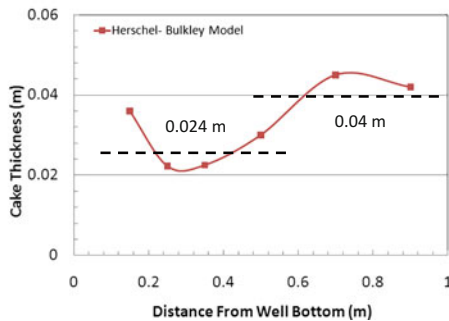
c) Filter cake thickness over well heights.

Fig. 4 a–c Deep drilling—filter cake thickness at different heights of wellbore from bottom. "Reprinted from *Asia-Pac. Journal of Chemical Engineering, 10, 809, 2015-Gamwo and Kabir*, with permission from John Wiley and Sons, September 12, 2016"

## 3.1 Deep Drilling Modeling and Simulation with Herschel–Bulkley Model

Figure 4a–c shows the simulated cake in the deep vertical wellbore wall for 45 µm particle drilling fluid. In this study, we have defined cake as solid volume fraction above 0.4 at the well wall. Figure 4a qualitatively shows filter cake thickness in half of the well with relatively thinner cake in the lower bottom part followed by thicker cake at the upper part of the well. Figure 4b shows solid volume fractions at different well heights from 0.25 to 0.5 m. Figure 4c displays the filter cake thickness extracted from the solid volume fraction graph, Fig. 4a. Figure 4c shows the cake thickness versus well heights. The average cake thickness varies from 0.024 m near the bottom well to 0.04 m near the top portion (Fig. 5c). This clearly implies that the simulated filter cake formed on the wellbore wall was non-uniform. These results agree qualitatively with the literature, which reports that non-uniform filter cake forms on the vertical porous media surface [34]. The non-uniformity of the filter cake is explained by the presence of vortices in the well annulus, which is discussed in the following section.

3.2 Comparison of Herschel–Bulkley Model with Power-Law Model

Figure 5a compares the steady-state drilling fluid path-lines for Herschel–Bulkley and power-law models. For both models, the expected fluid circulation pattern and intensity are observed with descending fluid flow in the pipe and ascending flow in the annulus. The down fluid flow magnitude is lower because the pressure drop is set to zero. The upflow magnitude is higher because the pressure drop is set to 500 psi (3.45 MPa). Compared to the power-law model, the Herschel–Bulkley model results exhibit higher magnitude of the ascending fluid velocity with significantly higher magnitude at the bottom to propel the debris. This will more efficiently transport cuttings to the surface. In addition, the Herschel–Bulkley model shows only two symmetrical vortices near the bottom of the pipe. The power-law model exhibits six vortices along the annulus section. These numerous vortices along the path of the ascending cuttings will hinder the debris removal process as the cuttings trapped in the vortices will tend to settle near the bottom rather than ascending to the surface. The accumulation of cuttings near the bottom hole may disrupt or prevent the rotation of the drill bit.

Figure 5b qualitatively compares the steady-state solid volume fraction deposited in the form of non-uniform filter cake on the wall for both models. It shows more uniform filter cake thickness for the Herschel–Bulkley model compared to the power-law model. This non-uniformity is probably induced by the numerous vortices along the annulus for the power-law model.

Herschel–Bulkley Model   Power-Law Model

Pathlines Colored by Velocity Magnitude (water) (m/s)
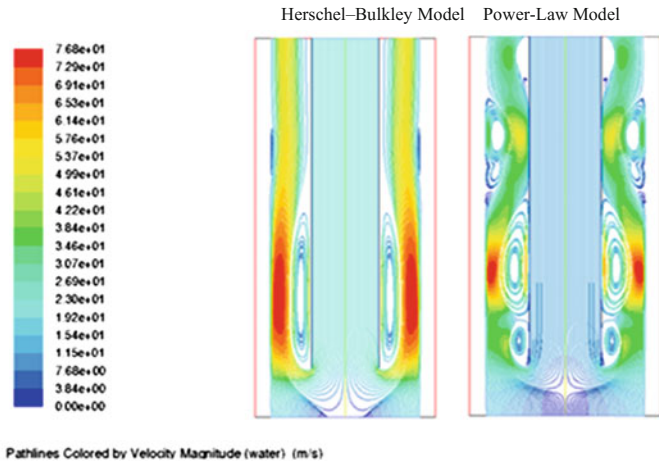
a) Pathlines Colored by Velocity Magnitude (m/s)


Solid Volume Fraction
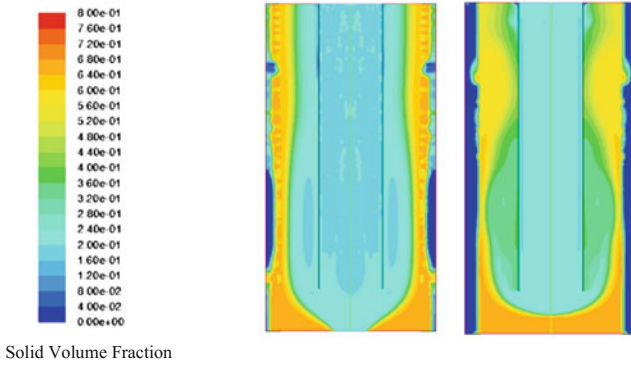
b) Qualitative solid fraction of vertical well (full).
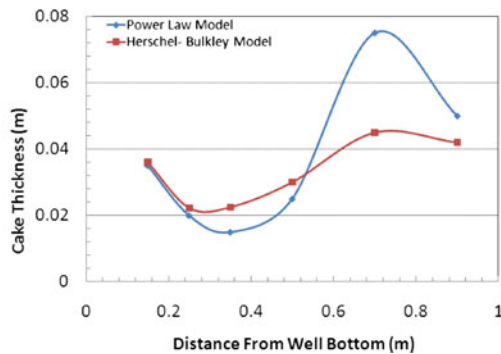
c) Filter cake thickness over well heights from bottom part.

Fig. 5 a–c Comparison of non-Newtonian fluid models on filter cake thickness. "Reprinted from *Asia-Pac. Journal of Chemical Engineering, 10, 809, 2015*-Gamwo and Kabir, with permission from John Wiley and Sons, September 12, 2016"

Figure 5c quantitatively displays filter cake thickness for Herschel–Bulkley and power-law models. It confirms the previous observation that the cake thickness is highly non-uniform when the fluid rheology is described by the power law. The numerous vortices are responsible for this non-uniformity. The average cake thickness at the bottom portion of the well is 0.024 m whereas the average cake thickness at the top part of the simulated well is 0.04 m for the Herschel–Bulkley model. However for power-law model, the average cake thickness at the bottom section of the well is 0.023 m while the average cake thickness at the top part of well is 0.05 m.
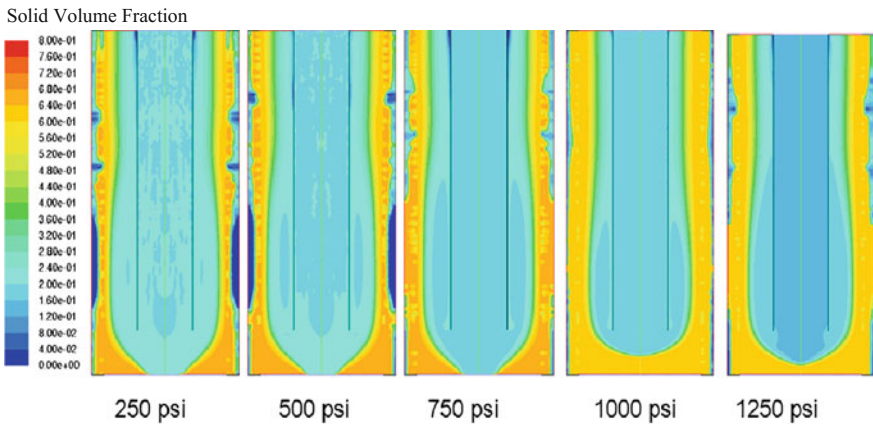
a) Qualitative filter cake and flow pattern at various differential pressures
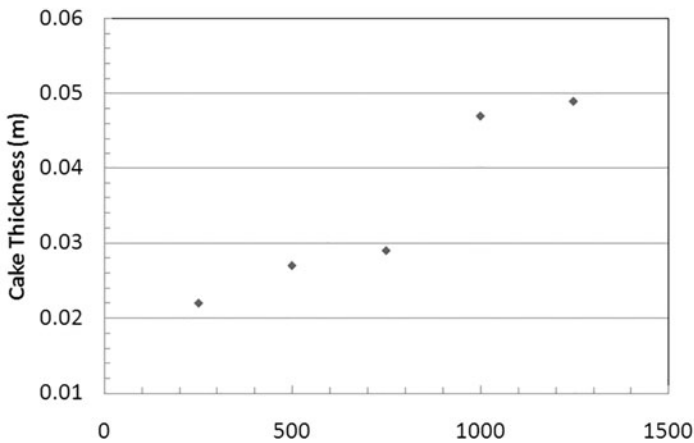
b) Cake thickness over differential pressure.

Fig. 6 a, **b** Effect of overbalance differential pressure on filter cake thickness for deep vertical well. "Reprinted from *Asia-Pac. Journal of Chemical Engineering, 10, 809, 2015-Gamwo and Kabir*, with permission from John Wiley and Sons, September 12, 2016"

3.3 Effect of Pressure on Flow Pattern and Filter Cake

To study the effect of overbalance differential pressure on cake thickness, CFD simulations were performed over a range of differential pressures, namely: 250 psi (or 1.72 MPa), 500 psi (or 3.45 MPa), 750 psi (or 5.17 MPa), 1000 psi (or 6.89 MPa), and 1250 psi (or 8.62 MPa). Their results are presented in Fig. 6a, b. Figure 6a qualitatively shows the filter cake pattern at various overbalance differential pressures in the well. As exhibited in the figure, cake thickness increases with increased pressure. The quantitative cake thicknesses were extracted from Fig. 6a and are presented in Fig. 6b, which clearly shows that the cake thickness increases with differential pressure as expected (Fig. 6a, b). Higher pressure forced more fluid into the formation by separating drilling fluid from a large number of solid particles and depositing these particles in the form of thicker cake on the wellbore wall.

Thicker cakes are not desirable because they often lead to drilling difficulties, such as stuck pipe and other drilling-related problems. Yet, extremely thin cake could lead to the loss of drilling fluid into the formation. Therefore, it is necessary to optimize filter cake thickness to achieve more efficient drilling. There is a paucity of experimental results for real-world deep drilling scenarios; therefore, these simulations would provide drilling engineers some guidelines on filter cake pattern and will also help engineers to optimize filter cake.

In addition to overbalance pressure, cake thickness also depends on several other parameters such as drilling fluid properties (density and viscosity), particle size and porosity of the formation.

4 Conclusions

The CFD numerical predictions were performed to mimic the extreme deep drilling process and cake formation in vertical wells located several miles beneath the Earth's surface. The CFD tool has successfully captured cake formation on the vertical subterranean zone during drilling and provided fluid flow patterns and velocity magnitudes of the drilling fluid during a deep drilling process.

Two sensitivity cases studies were carried out, one on the drilling fluid rheology model and one on the overbalance pressure drops. Their impacts on cutting removal performance have been inferred. The conclusions of this study are as follows:

- Two rheological models, the power-law and the Herschel–Bulkley model, were studied and both were able to predict the expected drilling fluid flow pattern at the bottom section of the deep drilling process with descending fluid in the pipe and ascending fluid in the annulus. Deviations were observed for the two models in the annulus ascending drilling fluid. The Herschel–Bulkley model predicted higher fluid and fewer vortices, indicating better removal of cuttings debris for rheological Herschel–Bulkley model fluids.

- The effect of overbalance pressure on filter cake thickness was investigated for five different overbalance pressures from 250 to 1250 psi. Cake thickness was found to increase linearly with the pressure drop. Based on this result, it is necessary to optimize the overbalance pressure when drilling for oil and gas at extremely high-temperature and high-pressure conditions, like those encountered miles underneath the Earth's surface. Such optimization of the overbalance pressure should improve the cuttings removal performance.

References

1. Ali, S. (2006). Reversible drilling-fluid emulsions for improved well performance. *Oilfield Review*.
2. Arthur, K. G., & Peden, J. M. (1988). The evaluation of drilling fluid filter cake properties and their influence on fluid loss. *SPE Journal*.
3. Berry, J. H. (2009). Drilling fluid properties & function, CETCO drilling products. Retrieved from http://www.getco.com.
4. Blkoor, S. O., & Fattah, K. A. (2013). The influence of xc-polymer on drilling fluid filter cake properties and formation damage. *Journal of Petroleum & Environmental Engineering*.
5. Cerasi, P., & Soga, K. (2001). Failure modes of drilling fluid filter cake. *Geotechnique, 51*(9), 777–785.
6. Cornelissena, J. T., Toghipour, F., Escudiéa, R., Ellisa, N., & Gracea, J. R. (2007). CFD modeling of a liquid–solid fluidized bed. *Chemical Engineering Science, 62,* 6334–6348.
7. Delhommer, H. J., & Walker, C. O. (1987). *Method for controlling lost circulation of drilling fluids with hydrocarbon absorbent polymer.* US Patent Number, 4:633,950.
8. Ding, J., & Gidaspow, D. (1990). A bubbling fluidization model using kinetic theory of granular flow. *Journal of A. I. Chemical Engineering, 36,* 523–538.
9. Fordham, E. J., Ladva, H. K. J., Hall, C., Baret, J. F., & Sherwood, J. D. (1988). Dynamic filtration of bentonite muds under different flow conditions. In *63rd Annual SPE Conference, Houston, Texas.*
10. Fisher, K. A., Wakeman, R. J., Chiu, T. W., & Meuric, O. F. J. (2008). Numerical modeling of cake formation and fluid loss from non-Newtonian mud's during drilling using eccentric/concentric drill strings with/without rotation. *Trans IChemE, 78 Part A,* 707–714.
11. Ferguson, C. K., & Klotz, J. A. (1954). Filtration from mud during drilling. *Trans AIME, 201,* 29–42.
12. Fluent. (2006). *FLUENT 6.3 User's Guide.* F. Inc. Lebanon, NH.
13. Fu, L. F., & Dempsey, B. A. (1998). Modeling the effect of particle size and charge on the structure of the filter cake in ultra-filtration. *Journal of Membrane Science, 149,* 221–240.
14. Gamwo, I. K., & Kabir, M. A. (2015). Impact of drilling fluid rheology and wellbore pressure on rock cuttings removal performance: Numerical investigation. *Asia-Pac. Journal of Chemical Engineering*.
15. Gidaspow, D., Bezburuah, R., & Ding, J. (1992). Hydrodynamics of circulating fluidized beds, kinetic theory approach. In *Fluidization VII, Proceedings of the 7th Engineering Foundation Conference on Fluidization.*

16. Hamed, S. B., & Belhadri, M. (2009). Rheological properties of biopolymers drilling fluids. *Journal of Petroleum Science and Engineering, 67,* 84–90.
17. Ishii, M. (1975). Thermo-fluid dynamic theory of two-phase flow. In *Collection de la Direction des Etudes et Recherches d'Electricite de France 22, Eyrolles. Paris.*
18. Jackson, R. (1997). Locally averaged equations of motion for a mixture of identical spherical particles and a Newtonian fluid. *Chemical Engineering Science, 52*(15), 2457–2469.
19. Johnson, P. C., Nott, P., & Jackson, R. (1990). Frictional–collisional equations of motion for participate flows and their application to chutes. *Journal of Fluid Mechanics, 210,* 501–535.
20. Johnson, P. C., & Jackson, R. (1987). Frictional-collisional constitutive relations for granular materials, with application to plane shearing. *Journal of Fluid Mechanics, 176,* 67–93.
21. Jung, J., & Gamwo, I. K. (2008). Multiphase CFD-based models for chemical looping combustion process: Fuel reactor modeling. *Powder Technology, 183,* 401–409.
22. Kabir, M. A., Khan, M. M. K., & Rasul, M. G. (2004). Flow of a low concentration polyacrylamide fluid solution in a channel with a flat plate obstruction at the entry. *Korea-Australia Rheology Journal, 16*(2), 63–73.
23. Kabir, M. A., Khan, M. M. K., & Rasul, M. G. (2013). Reverse flow phenomena of a polyacrylamide solution in a channel with an obstacle at the entry: Influence of obstruction geometry. *Journal of Chemical Engineering Communications, 199*(4), 1–20.
24. Kabir, M. A., & Gamwo, I. K. (2011). Filter cake formation on the vertical well at high temperature and high pressure: Computational fluid dynamics modeling and simulations. *Journal of Petroleum and Gas Engineering, 2*(7), 146–164.
25. Kelsey, J. R., & Carson, C. C. (1987). Geothermal drilling-drilling for geothermal energy. *Geothermal Sciences and Technology, 1,* 39–61.
26. Lun, C. K. K., Savage, S. B., Jerey, D. J., & Chepurniy, N. (1984). Kinetic theories for granular flow: Inelastic particles in Couette flow and slightly inelastic particles in a general flow field. *Journal of Fluid Mechanics, 140,* 223–256.
27. Maurer Engineering Inc. (1997). *Wellbore thermal simulation model: Theory and user's manual.* Maurer Engineering Inc.
28. Myöhänen, K., Hyppänen, T., & Kyrki-Rajamäki, R. (2006). *CFD modeling of fluidized bed systems.* Finland: SIMS.
29. Outmans, H. D. (1963). Mechanics of static and dynamic filtration in the borehole. *SPE, 228*(236).
30. Peden, J. M., Avalos, M. R., & Arthur, K. G. (1982). The analysis of the dynamic filtration and permeability impairment characteristics of inhibited water based muds. In *SPE Formation Damage Control Symposium, Lafayette.*
31. Parn-anurak, S. (2003). *Modeling of fluid filtration and near-wellbore damage along a horizontal well.* Ph.D. thesis, New Mexico Institute of Mining and Technology, USA.
32. Rogers, H. E., Murray, D. A., & Webb, E. D. (1996). *Apparatus and method for removing gelled drilling fluid and filter cake from the side of a wellbore.* US Patent 5564,500.
33. Saha, H. (2009). *Practical application of filtration theory to the minerals industry.* Ph.D. Thesis, The University of Melbourne, Australia.
34. Sherwood, J. D., Meeten, G. H., Farrow, C. A., & Alderman, N. J. (1991). Squeeze-film rheometry of non-uniform mudcak. *Journal of Non-Newtonian Fluid Mechanics, 39,* 311–334.
35. Sherwood, J. D., Meeton, G. H., Farrow, C. A., & Alderman, N. J. (1991). Concentration profile within non-uniform mudcakes. *Journal* of the *Chemical Society, Faraday* Transactions, *84*(4), 611.
36. Spooner, K. M., Bilbo, D., & McNeil, B. (2004). The application of high temperature polymer drilling fluid on Smackover operations in Mississippi. In *AADE-2004 Drilling Fluids Conference, Houston, Texas.*
37. Usher, S. P., Kretser, R. G., & Scales, P. J. (2001). Validation of a new filtration technique for de-waterability characterization. *AIChE Journal, 47*(7), 1561–1570.

38. Vaussard, A., Martin, M., Konirsch, O., & Patroni, J. M. (1986). An experimental study of drilling fluids dynamic filtration. In *SPE 61st Annual Technical Conference, New Orleans*.
39. Warren, B. K., Smith, T. R., & Ravi, K. M. (1993). Static and dynamic fluid-loss characteristics of drilling fluids in a full-scale wellbore. *SPE Journal*.
40. Wikipedia. (2010). Oil well. Retrieved from http://en.wikipedia.org/wiki/oil_well.well.